PNAS RESEARCH ARTICLE | MICROBIOLOGY

The helicase-like transcription factor redirects the autophagic flux and restricts human T cell leukemia virus type 1 infection

Aurélie Beauvois[a,b,1,2], Hélène Gazon[a,b,1], Pradeep Singh Chauhan[a,b], Majeed Jamakhani[a,b], Jean-Rock Jacques[a,b], Marc Thiry[c], Emmanuel Dejardin[d], Emmanuel Di Valentin[e], Jean-Claude Twizere[f], Jean-Marie Péloponèse[g], Makon-Sébastien Njock[h], Jun-Ichirou Yasunaga[i], Masao Matsuoka[i], Malik Hamaïdia[a,b,1], and Luc Willems[a,b,1,2]

Edited by Robert Gallo, University of Maryland School of Medicine, Baltimore, MD; received September 21, 2022; accepted May 11, 2023

Retroviruses and their host have coevolved in a delicate balance between viral replication and survival of the infected cell. In this equilibrium, restriction factors expressed by infected cells control different steps of retroviral replication such as entry, uncoating, nuclear import, expression, or budding. Here, we describe a mechanism of restriction against human T cell leukemia virus type 1 (HTLV-1) by the helicase-like transcription factor (HLTF). We show that RNA and protein levels of HLTF are reduced in primary T cells of HTLV-1-infected subjects, suggesting a clinical relevance. We further demonstrate that the viral oncogene Tax represses HLTF transcription via the Enhancer of zeste homolog 2 methyltransferase of the Polycomb repressive complex 2. The Tax protein also directly interacts with HLTF and induces its proteasomal degradation. RNA interference and gene transduction in HTLV-1-infected T cells derived from patients indicate that HLTF is a restriction factor. Restoring the normal levels of HLTF expression induces the dispersal of the Golgi apparatus and overproduction of secretory granules. By synergizing with Tax-mediated NF-κB activation, physiologically relevant levels of HLTF intensify the autophagic flux. Increased vesicular trafficking leads to an enlargement of the lysosomes and the production of large vacuoles containing viral particles. HLTF induction in HTLV-1-infected cells significantly increases the percentage of defective virions. In conclusion, HLTF-mediated activation of the autophagic flux blunts the infectious replication cycle of HTLV-1, revealing an original mode of viral restriction.

HTLV-1 | HLTF | restriction factors | intrinsic immunity | Tax

Significance

Over time, retroviruses evolved the ability to exploit cellular pathways to promote their life cycle. In turn, host cells have developed restriction factors to control different steps of retroviral replication. Here, we describe a mechanism of restriction against human T cell leukemia virus type 1 (HTLV-1) by the helicase-like transcription factor (HLTF). HLTF fragments the Golgi apparatus and enlarges lysosomes in HTLV-1-infected cells, leading to budding of defective virions. As the HIV, HLTF-mediated restriction also occurs at early and late steps of HTLV-1 infection. This report thus reveals that HLTF interferes with different steps of the infectious cycle of the two retroviruses consistent with specificities in their mode of replication.

As obligate intracellular parasites, viruses use the host cell machinery to persist and replicate (1, 2). Viruses and their host have coevolved in a delicate balance between viral replication and survival of the infected cell. This fine-tuned equilibrium is notably mediated by the interaction of viral and cellular factors that govern the host immune response (3–6). Besides innate and adaptive immunity, restriction factors are antiviral proteins that control different steps of the virus replication cycle. Restriction factors interfere with virus entry and cell fusion (e.g., IFITM1, IFITM3/2, SERINC5), uncoating (TRIM5α), nuclear import (MxB), genome replication (APOBEC, SAMHD1, and MxA), viral transcription, translation or protein synthesis (CIITA), and virion release (BST-2) (3–6). Viruses express proteins counteracting the activities of these restriction factors as exemplified in the case of HIV-1 by Nef, Vif, and Vpu that inhibit SERINC5 (5), APOBEC3G (7), and BST-2 (8, 9), respectively.

Although the mechanisms may differ among viruses (e.g., sequestration), the antiviral proteins primarily target the restriction factor for proteasomal or lysosomal degradation. This proteolysis is mediated by polymerization of K48- or K63-linked ubiquitin chains (5). Ubiquitin E3 ligases and deubiquitinating enzymes (DUBs) are notably recruited to the Golgi apparatus and regulate the intracellular trafficking of proteins (10). Besides proteolysis associated with the endoplasmic reticulum, ubiquitinated proteins can be directly degraded by proteasomes bound to the Golgi membranes. For example, this process involves ubiquitination of the structural Golgi protein (GM130) in response to Golgi stress and its subsequent proteolysis in the proteasome. This Golgi apparatus–related degradation (GARD) thus allows the Golgi to quickly regulate its morphology in response to stress. Alternatively, ubiquitinated proteins can be trapped in autophagosomes and undergo vesicular trafficking (11). The autophagosomes then either fuse with lysosomes or migrate to the plasma membrane via the endosomal system (12). If not degraded in autophagolysosomes, proteins will bind to the plasma membrane and will be secreted into the extracellular milieu (13).

Author contributions: M.H. and L.W. designed research; A.B., H.G., P.S.C., M.T., E.D.V., J.-C.T., and J.-M.P. performed research; J.-R.J., E.D., M.-S.N., J.-I.Y., and M.M. contributed new reagents/analytic tools; A.B., H.G., P.S.C., M.J., M.T., and M.H. analyzed data; and A.B. and L.W. wrote the paper.

The authors declare no competing interest.

This article is a PNAS Direct Submission.

[1]A.B., H.G., M.H. and L.W. contributed equally to this work.

[2]To whom correspondence may be addressed. Email: aurelie.beauvois@uliege.be or luc.willems@uliege.be.

This article contains supporting information online at https://www.pnas.org/lookup/suppl/doi:10.1073/pnas.2216127120/-/DCSupplemental.

Published July 24, 2023.

Vesicular trafficking and autophagy have been subverted by a number of viruses (11). Among these, the human T cell leukemia virus type 1 (HTLV-1) encodes the Tax oncoprotein. The Tax oncoprotein is a master regulator of cellular gene transcription by signaling through three main pathways (ATF/CREB, NF-κB, and SRF) (14–16). Tax affects vesicular trafficking by promoting autophagosome formation and inhibiting fusion with lysosomes (17, 18). The regulatory mechanisms mediated by Tax appear to be quite complex but involve at least in part the activity of several ubiquitin-modifying enzymes and activation of the NF-κB pathway. HTLV-1 Tax stimulates the assembly of K63-linked polyubiquitin chains by RNF8 followed by a TAK1-dependent IKK activation (19). Tax can also induce the generation of Lys63- and Met1-linked hybrid polyubiquitin chains (20). The Tax protein itself is ubiquitinated by the E3/E4 ubiquitin conjugation factor UBE4B, promoting NF-κB activation (21). The autophagic receptor protein p62 potentiates Tax activity in cells by facilitating the association of ubiquitin chains with the Tax/IKK signalosome (22). Collectively, these observations thus indicate that ubiquitination, NF-κB activation, and autophagy are tightly regulated by Tax. Promotion of autophagy at the expense of lysosomal proteolysis is believed to be a major step in HTLV-1 infectivity (12).

In this study, we show that the helicase-like transcription factor (HLTF), an E3 ubiquitin ligase, is down-regulated in T cells from HTLV-1-infected subjects. HLTF belongs to the SWI/SNF family of chromatin remodelers and mediates DNA damage tolerance pathways. Here, we demonstrate that HLTF is a restriction factor that reduces HTLV-1 transmission both at early and late steps of the viral life cycle.

Results

Helicase-Like Transcription Factor (HLTF) Expression Is Down-Regulated in HTLV-1-Associated Myelopathy/Tropical Spastic Paraparesis (HAM/TSP) and Adult T Cell Leukemia (ATL). This study was initiated as a follow-up to RNA sequencing and microarray datasets indicating that *HLTF* expression was dysregulated in ATL patients compared to healthy donors (*SI Appendix*, Fig. S1). To validate these transcriptomic analyzes, the levels of *HLTF* mRNAs were quantified by RT-qPCR in CD8+ depleted peripheral blood mononuclear cells (PBMCs) from HTLV-1-infected subjects. Clinical and pathological information about HTLV-1 samples is described in *SI Appendix*, Table S2. Consistently with previous reports, *tax* expression was significantly up-regulated in HAM/TSP compared to asymptomatic carriers (AC) and ATLs (Fig. 1*A*) (23–25). In contrast, the levels of the HTLV-1 bZIP factor (*HBZ*) mRNAs were increased in ATLs confirming previous findings of an inverse correlation with *tax* transcription (Fig. 1*B*) (26, 27). In this series of 60 HTLV-1-infected subjects, *HLTF* expression was significantly down-regulated in TSP/HAM and ATLs compared to AC and noninfected healthy donors (HD) (Fig. 1*C*). Note that a limitation of these analyses was the presence of monocytes and B cells in addition to CD4+ T cells. Therefore, these data might not reflect the expression level in HTLV-1-infected cells and ATL cells since the percentage of HTLV-1-infected CD4+ T cells in AC and TSP was lower than that in ATL cases. Interestingly, *HLTF* transcription was even completely undetectable by RT-qPCR in 13 out of 20 ATL cases. Considering the transcription levels in each sample individually, the expression levels of *tax* and *HLTF* were inversely correlated in ATL (ρ=−0.71, P=0.00043; Fig. 1*D*). ATL samples that were completely negative for *tax* transcripts thus contained higher levels of *HLTF* RNA. Furthermore, flow cytometry analysis with two representative ATL samples able to express Tax (ATL#1) or not (ATL#2) indicated that the mean fluorescence intensity (MFI) of HLTF was reduced (MFI 634 *vs* 963), illustrating a negative correlation with Tax (MFI 418 *vs* 240), respectively (Fig. 1*E*). These RT-qPCR and flow cytometry analyzes thus showed that HLTF was down-regulated in ATL. *HLTF* transcription was also significantly reduced in a series of HTLV-1-infected lymphocytes (C8166, C91PL, MT4, HuT102, and MT2) compared to control T cell lines (CEM, MOLT4, KIT-225, and Jurkat) (Fig. 1*F*). Analysis of RNAseq datasets further demonstrated that *HLTF* transcription was lower in primary T cell populations than in Jurkat and KIT-225 (*SI Appendix*, Fig. S2). In particular, an HTLV-1-infected cell line derived from a patient with cutaneous T cell lymphoma (HuT102) was devoid of detectable *HLTF* mRNAs as observed in a proportion of ATL samples. Reduced expression of HLTF protein was confirmed by immunoblot (Fig. 1*G*). Quantification of Tax and HLTF proteins indicated that their levels were inversely correlated (Fig. 1*H*). Using a doxycycline-inducible system, HLTF expression was slightly increased in two HTLV-1-infected cell lines (2.5-fold in MT2-iHLTF and 2-fold in C91PL-iHLTF) (Fig. 1*I*). In the presence of doxycycline, the levels of the HLTF protein (i.e., 0.5-0.6 band luminescence intensities relative to tubulin, RLU) remained below the physiological range of the Jurkat control (0.9 RLU). Upon HLTF induction, Tax expression was not significantly affected in the two cell lines. In contrast, induction of Tax expression with zinc chloride ($ZnCl_2$) in JPX-9 T lymphocytes correlated with a reduction of HLTF protein (RLU from 0.9 to 0.6; Fig. 1*J*).

These data demonstrate that HLTF is down-regulated both at the transcriptional and translational levels in HTLV-1-infected cell lines as well as in primary lymphocytes from HAM/TSP and ATL patients.

HLTF Transcription is Repressed by Promoter Cytosine Methylation and by the Enhancer of Zeste Homolog 2 (EZH2) Methyltransferase. Besides activating transcription (14–16), Tax also mediates gene repression via the EZH2 H3K27me3 methyltransferase of the Polycomb Repressive Complex 2 (PRC2) (28). To investigate whether this mechanism applies to *HLTF* transcription, Tax expression was induced with $ZnCl_2$ in JPX-9 T lymphocytes, and chromatin immunoprecipitation (ChIP) of the *HLTF* promoter was performed with EZH2-specific antibodies. Results of *SI Appendix*, Fig. S3 indicated that Tax hijacks EZH2 to induce trimethylation of H3K27 on the CpG region of the *HLTF* promoter, leading to the inhibition of *HLTF* transcription.

The *HLTF* gene also appeared to be silenced by cytosine methylation. Indeed, treatment of HuT102 cells with 5-aza-dC increased transcription of *HLTF* (*SI Appendix*, Fig. S4), revealing a mechanism of epigenetic repression by DNA methylation of the *HLTF* promoter. This mechanism may also explain *HLTF* transcriptional silencing in a proportion of ATL samples in which *tax* RNA is absent.

Tax Interacts with and Induces Proteasomal Degradation of HLTF. Transient induction of Tax expression in JPX-9 T lymphocytes mitigated the amounts of HLTF protein (Fig. 1*J*). To further explore the interaction between these two proteins, the presence of HLTF in the Tax complex was investigated in Hek293T cells via the Gaussia princeps Complementation Assay (GPCA) (29). In this system, Tax and HLTF were fused to complementary and inactive fragments of the *Gaussia princeps* luciferase enzyme (Fig. 2*A*). After cotransfection of the recombinant plasmids (i.e., pSPICA-N1-Tax with pSPICA-N2-HLTF and pSPICA-N2-Tax with pSPICA-N1-HLTF) into Hek293T, the interaction between Tax and HLTF restored luciferase activity (TaxN2+HLTFN1 and TaxN1+HLTFN2; Fig. 2*B*). The Tax/HLTF interaction was then evaluated by a coimmunoprecipitation

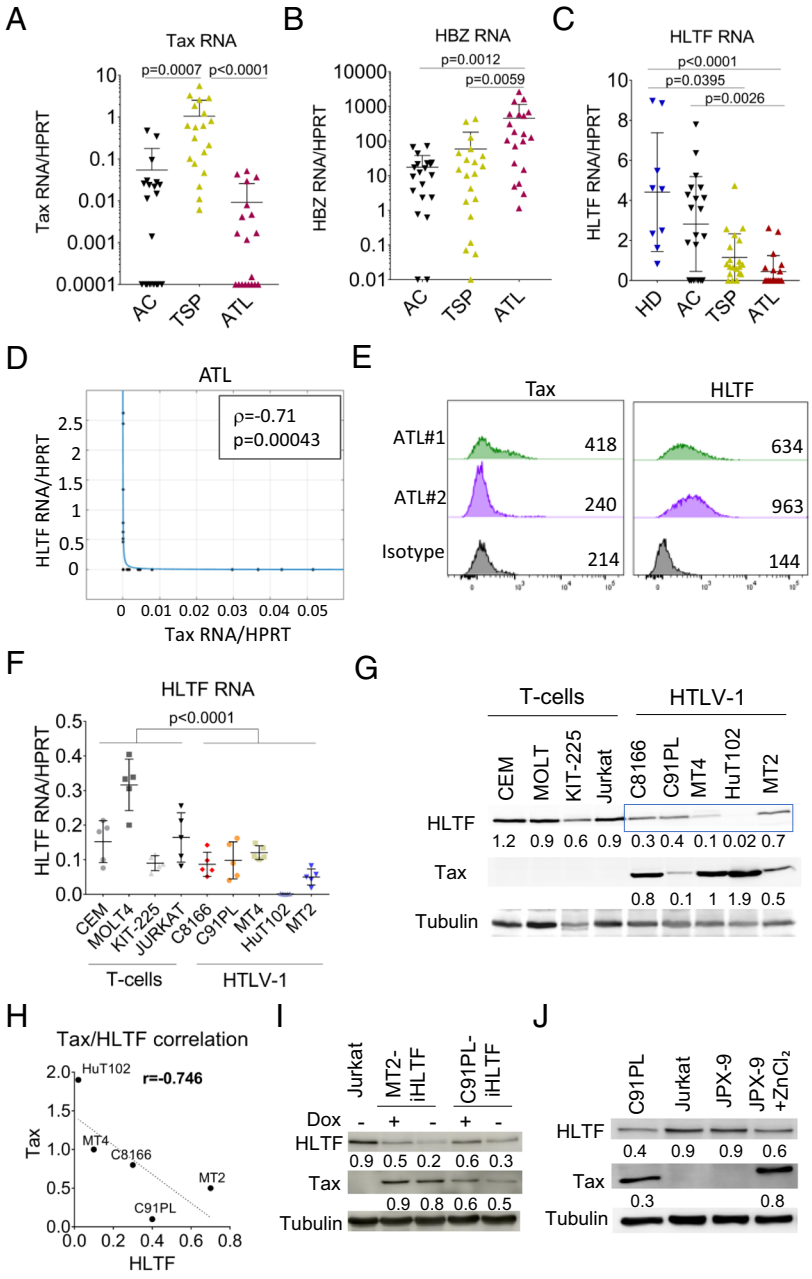

Fig. 1. HLTF is down-regulated in primary lymphocytes from HTLV-1-infected subjects and patient's derived cell lines. (*A–C*) RT-qPCR quantification of *tax*, *HBZ*, and *HLTF* RNAs from nine healthy donors (HDs), HTLV-1-infected asymptomatic carriers (ACs; n = 20), and patients with tropical spastic paraparesis (TSP; n = 20) or with acute adult T cell leukemia (ATL; n = 20). Dunn's multiple comparison tests were used to determine statistically significant differences between groups. (*D*) Nonlinear regression of *tax* and *HLTF* RNA levels in ATL samples was performed with the curve fitting function of Matlab. ρ represents the Spearman correlation between *tax* and *HLTF*. (*E*) The MFI of Tax and HLTF was quantified by flow cytometry in 2 ATL samples (ATL#1 and ATL#2). After labeling with the corresponding primary antibodies, Tax and HLTF were fluorescently revealed with Alexa Fluor 488 and Alexa Fluor 647 conjugates, respectively. An isotype antibody was used as control. The numbers indicate the MFI. (*F*) RT-qPCR quantification of *HLTF* in HTLV-1-infected T cell lines (C8166, C91PL, MT4, HuT102, and MT2) and control T lymphocytes (CEM, MOLT4, KIT-225, and Jurkat). RT-qPCR data are presented as mean ± SD of at least five independent experiments. A Mann–Whitney test was used to determine the statistical significance of the difference between HTLV-1-infected and control cell lines. (*G*) Western blot analysis of HLTF and Tax proteins in HTLV-1-infected and control cell lines. Numbers in immunoblots indicate the band intensities of HLTF and Tax normalized to tubulin. (*H*) Pearson correlation analysis between Tax and HLTF normalized band intensities. (*I*) Western blot analysis of HLTF and Tax proteins in MT2 and C91PL cells transduced with a doxycycline-inducible HLTF expression system (MT2-iHLTF and C91PL-iHLTF). (*J*) Western blot analysis of HLTF and Tax levels in JPX-9 cells after induction of Tax with $ZnCl_2$.

assay in JPX-9 T lymphocytes (Fig. 2*C*). After induction of Tax expression with $ZnCl_2$ in JPX-9 cells and immunoprecipitation with an anti-Tax antibody, immunoblotting revealed the presence of HLTF in the protein complex (Fig. 2*C*). Coimmunoprecipitation thus indicated that Tax complexes with HLTF in T cells. This conclusion was also valid in HTLV-1-infected cells (C91PL, Fig. 2*D*) and in HuT102 transduced with an HLTF-inducible lentivector (HuT102-iHLTF+dox; Fig. 2*E*).

To determine the biological relevance of the interaction, the colocalization of Tax and HLTF was investigated by confocal microscopy in HTLV-1 immortalized C91PL cells. Tax and HLTF were mainly colocalized in regions surrounding the nucleus (red arrows on colocalization Tax/HLTF; Fig. 2*F*). Quantification of the fluorescence intensities in two representative cells nevertheless highlighted a broad diversity in the expression profiles (Fig. 2*G*). When HLTF protein levels were induced by 1.9-fold in doxycycline-inducible

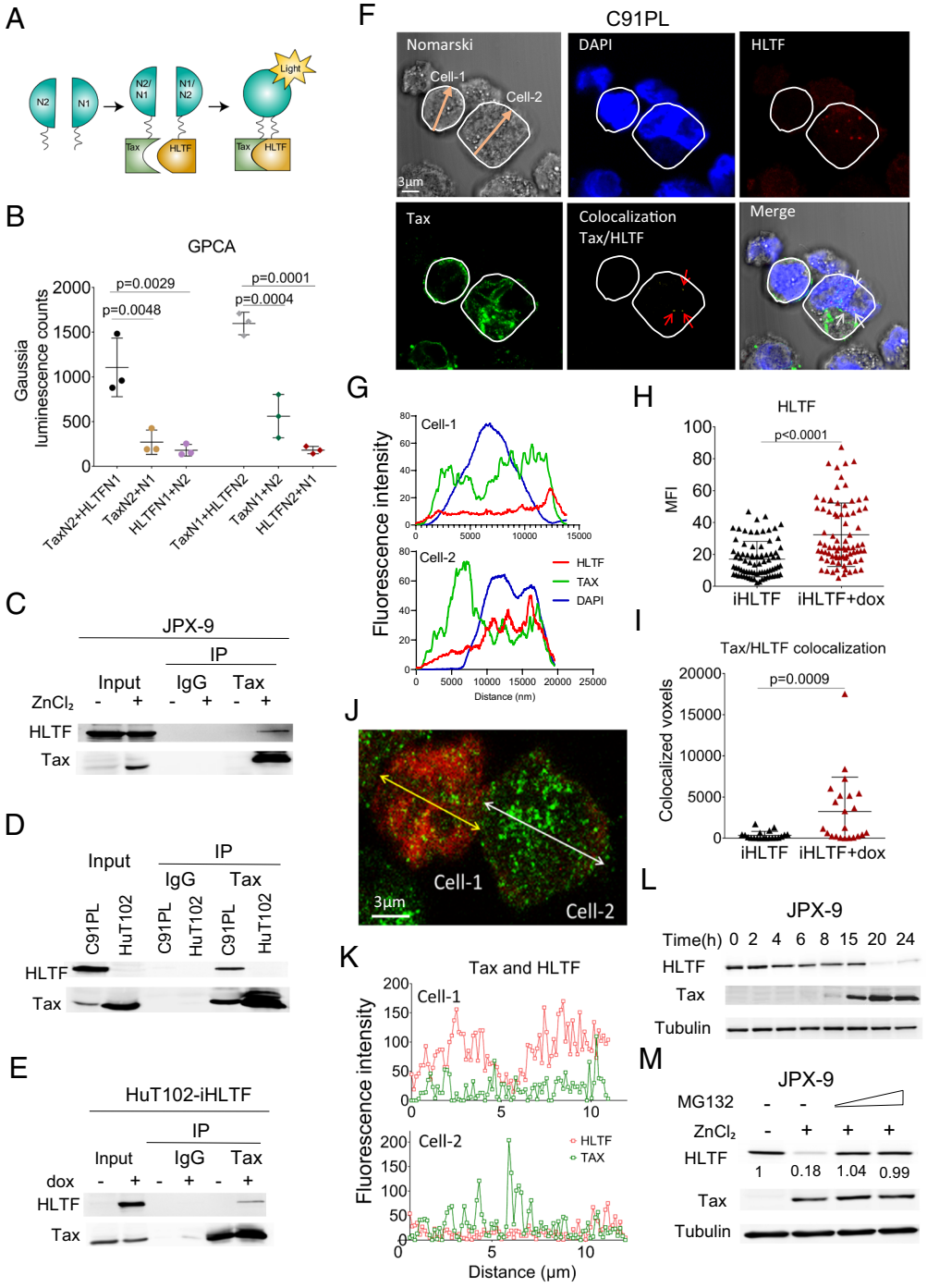

Fig. 2. Tax protein physically interacts with HLTF protein in HTLV-1-infected T cells and induces its depletion via proteasome degradation. (*A*) Schematic representation of the GPCA assay. Tax and HLTF were fused to complementary and inactive fragments of the *Gaussia princeps* luciferase enzyme (i.e., pSPICA-N1 and pSPICA-N2 are referred to as N1 and N2, respectively). If Tax and HLTF interact, the enzymatic activity of the luciferase is restored, resulting in light emission. (*B*) Luciferase activity in Hek293T cells coexpressing Tax and HLTF (i.e., Tax-N1 with HLTF-N2 and Tax-N2 with HLTF-N1) or coexpressing each partner with matched empty plasmid (i.e., Tax-N1 with N2, HLTF-N2 with N1, Tax-N2 with N1, and HLTF-N1 with N2). Data are the mean (±SD) of three independent experiments. *P* values were calculated according to the Dunnett's multiple comparison test (*C*) Coimmunoprecipitation analysis of the Tax/HLTF interaction in JPX-9 cells after induction of Tax. Tax immunoprecipitates were analyzed by western blot using anti-HLTF antibody. (*D*) Coimmunoprecipitation analysis of the Tax/HLTF interaction in C91PL and HuT102 HTLV-1 infected cells using an anti-Tax antibody. Tax immunoprecipitates were analyzed by western blot using an anti-HLTF antibody. (*E*) Immunoprecipitation of HLTF in HuT102-iHLTF cells using an anti-Tax antibody 48 h after induction with doxycycline. (*F*) Confocal analysis of the colocalization between Tax (green, Alexa Fluor 488) and HLTF (red, Alexa Fluor 647) in C91PL cells. Voxel colocalization (small red arrows) was determined using software Zen Blue and Imaris. The colocalization threshold was set manually. (*G*) The fluorescence intensities of Tax (green) and HLTF (red) in two C91PL cells (Cell-1 and Cell-2) were quantified along the arrows shown in the Nomarski image of panel *F*. (*H*) Mean fluorescent intensity (MFI) of HLTF in C91PL-iHLTF after induction of HLTF with doxycycline (iHLTF+dox). The *P* value was calculated according to the Mann–Whitney test. (*I*) Quantification of Tax/HLTF colocalized voxels in C91PL-iHLTF after induction of HLTF with doxycycline. The *P* value was calculated according to the Mann–Whitney test. (*J*) Confocal microscopy after labeling of Tax (green, Alexa Fluor 488) and HLTF (red, Alexa Fluor 647) in MT2 cells. (*K*) The fluorescence intensities of Tax (green) and HLTF (red) in two MT2 cells (Cell-1 and Cell-2) were quantified along the double arrow lines shown in panel *J*. (*L*) HLTF and Tax protein levels were quantified by western blot at 0–4–6–8–15–20–24 h after induction of Tax expression with $ZnCl_2$ in JPX-9 cells. (*M*) Western blot analysis of Tax and HLTF levels in Tax-induced JPX-9 cells. After Tax induction, JPX-9 cells were treated with the MG132 proteasome inhibitor for 6 h (the two lanes below the triangle correspond to 20 µM and 30 µM MG132). Numbers in immunoblots indicate the quantification of band intensities of HLTF and Tax normalized to tubulin.

C91PL-iHLTF cells (Fig. 2*H*), Tax/HLTF colocalization significantly increased (Fig. 2*I*). Two other HTLV-1 infected cell lines (MT2 and HuT102) displayed a similar heterogeneity in Tax expression as well as in Tax/HLTF colocalization (*SI Appendix*, Figs. S5 and S6). Multiple labeling of different cell compartments (nucleus, cytoskeleton, and cis-Golgi) validated the spatial colocalization of Tax and HLTF (*SI Appendix*, Fig. S7). The voxel profiles nevertheless revealed a bimodal distribution characterized by a proportion of events almost completely devoid of colocalization. In other words, the expression of Tax and HLTF was mutually exclusive in a subpopulation of HTLV-1-infected cells, as illustrated in MT2 cells (Fig. 2*J*). Profiling of the fluorescence intensity quantified this observation along the double arrows (Cell-1 and Cell-2; Fig. 2*K*). The most likely hypothesis of this phenotype is that Tax, whose expression fluctuates in HTLV-1 infected cells (27, 30), degrades HLTF in the proteasome (31). Consistently, induction of Tax expression decreased the protein levels of HLTF in JPX-9 cells (Fig. 2*L*). Involvement of the proteasomal degradation was validated by using the MG132 inhibitor that blocks the proteolytic activity of the 26S complex (Fig. 2*M*).

Based on the opposite effects of Tax and another viral factor (HBZ), similar experiments were undertaken to evaluate their combined activity on HLTF expression. Induction of HBZ expression in JPX-9 T lymphocytes affected neither HLTF protein levels (*SI Appendix*, Fig. S8 *A–C*) nor interactions with Tax (*SI Appendix*, Fig. S8*D*). Furthermore, gene transduction of HBZ into MT2 or C91PL did not modify HLTF transcription and protein levels (*SI Appendix*, Fig. S8 *E–J*).

Together, these results show that the Tax oncoprotein interacts with and depletes HLTF in the proteasome.

HLTF Is a Restriction Factor. The targeted degradation in the proteasome (Fig. 2) combined with transcriptional repression (Fig.1 and *SI Appendix*, Fig. S3) of HLTF by the Tax oncoprotein suggests an important role in the life cycle of HTLV-1. To address viral infectivity, HLTF expression levels were modulated by RNA interference and gene transduction in HTLV-1-infected lymphocytes. Special attention was given to the biological relevance of the cell model based on human lymphocytes derived from patients and on physiological levels of HLTF. These conditions were achieved in two HTLV-1 cell lines (MT2 and C91PL) using RNA interference (shHLTF) and transduction of a doxycycline-inducible expression system (iHLTF) (Fig. 3). To quantify the predominant mode of cell-to-cell infection, MT2 and C91PL were cocultured with Jurkat-luc reporter T cells containing a luciferase gene controlled by the HTLV-1 LTR viral promoter (32) (Fig. 3*A*). Compared to the scrambled control, interference with the shHLTF lentivector reduced *HLTF* transcription in the two HTLV-1-infected cell lines (Fig. 3 *B* and *D*) but only marginally affected *tax* RNA levels (*SI Appendix*, Fig. S9). Concomitantly, RNA interference with HLTF increased luciferase reporter activity upon coculture with Jurkat-luc cells (Fig. 3 *F* and *H*). In contrast, induction of HLTF expression in C91PL (Fig. 3*C*) and MT2 (Fig. 3*E*) by gene transduction (iHLTF vs iHLTF+dox) did not affect *tax* RNA (*SI Appendix*, Fig. S9) but reduced luciferase activity (Fig. 3 *G* and *I*).

This standard infectivity assay suggests that HLTF interferes with HTLV-1 transmission to Jurkat-luc T lymphocytes and acts as a restriction factor without impacting Tax expression. A similar conclusion was drawn when HLTF expression was modulated directly in the Jurkat-luc cells instead of in the HTLV-1-infected lymphocytes (*SI Appendix*, Fig. S10). HLTF therefore restricts HTLV transmission both in the donor and in the acceptor cell (i.e., persistently infected and target cell, respectively)

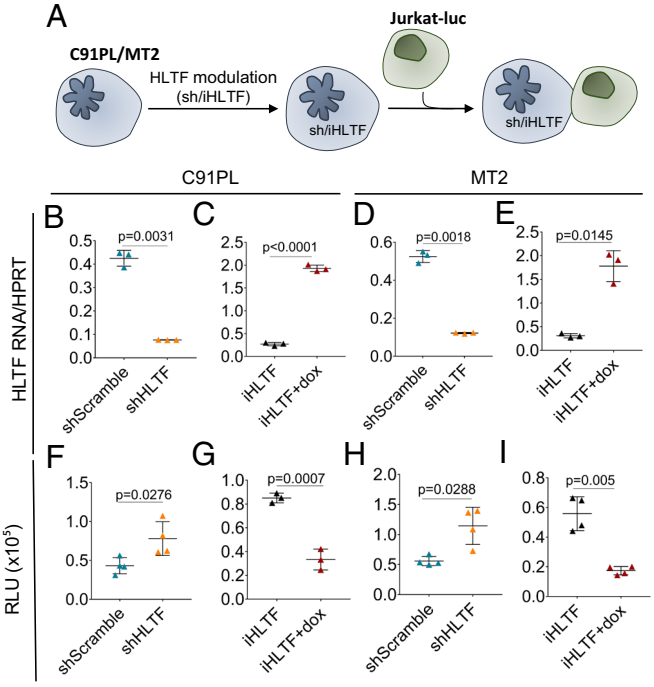

Fig. 3. HLTF is a restriction factor in C91PL and MT2 cells persistently infected with HTLV-1. (*A*) Schematic representation of the infectivity assay. HLTF expression was modulated by RNA interference (shHLTF) or gene transduction (iHLTF) in MT2 and C91PL HTLV-1-infected cells. MT2-shHLTF, MT2-iHLTF, C91PL-shHLTF, and C91PL-iHLTF cells were then cocultured at a 5/1 ratio with Jurkat-luc lymphocytes containing a stably integrated luciferase gene controlled by the LTR promoter. (*B–E*) Quantification of *HLTF* RNAs by RT-qPCR in MT2-shHLTF, MT2-iHLTF, C91PL-shHLTF, and C91-iHLTF cells. MT2 and C91PL cells transduced with a scramble shRNA were used as control. Analysis was performed 48 h after induction of HLTF expression with doxycycline (+dox). (*F–I*) Quantification of luciferase activity in cocultures of MT2-shHLTF, MT2-iHLTF, C91PL-shHLTF, or C91PL-iHLTF with Jurkat-luc reporter lymphocytes. Relative luminescence units (RLU) data are presented as the mean (±SD) of at least three independent experiments. *P* values were calculated according to the *t* tests.

HLTF Increases Vesicle Production in HTLV-1-Infected Cells. As a member of the SWI/SNF chromatin remodelers, HLTF may affect HTLV-1 transcription and indirectly reduce HTLV-1 infectivity. Experiments described in *SI Appendix*, Fig. S11 invalidated this trivial hypothesis.

To further characterize the mechanism of restriction, the subcellular localization of HLTF was identified by confocal microscopy. Since HTLV-1-infected lymphocytes naturally express low amounts of HLTF (Fig. 1 *A–H*), the doxycycline-inducible system was implemented to increase its protein levels in MT2 cells (i.e., from 0.2 to 0.5 compared to 0.9 in Jurkat; Fig. 1*I*). HLTF localized in punctate areas of the nucleus consistently with its involvement in mechanisms of tolerance to DNA damage (33). However, most HLTF proteins colocalized with Tax and the cis-Golgi matrix protein GM130 (Fig. 4*A*). In HTLV-1-infected MT2 cells, large aggregates containing HLTF, Tax, and GM130 polarized upon cell-to-cell contact. Induction of HLTF with doxycycline decreased the mean fluorescence intensity (MFI) of Tax in the cis-Golgi as identified by the GM130 marker (Fig. 4*B*). Furthermore, the volume of the cis-Golgi apparatus was considerably reduced in the presence of HLTF (Fig. 4 *C* and *D*). As a control, doxycycline did not affect the Golgi apparatus in parental MT2 cells that were not transduced with the lentiviral HLTF expression system (Fig. 4*D*). Similar experiments in C91PL cells broadened these observations to another HTLV-1-infected cell line, further supporting the role of HLTF in shrinkage of the cis-Golgi apparatus (*SI Appendix*, Fig. S12). Deeper insight into the organelle structure by transmission electron microscopy revealed that the

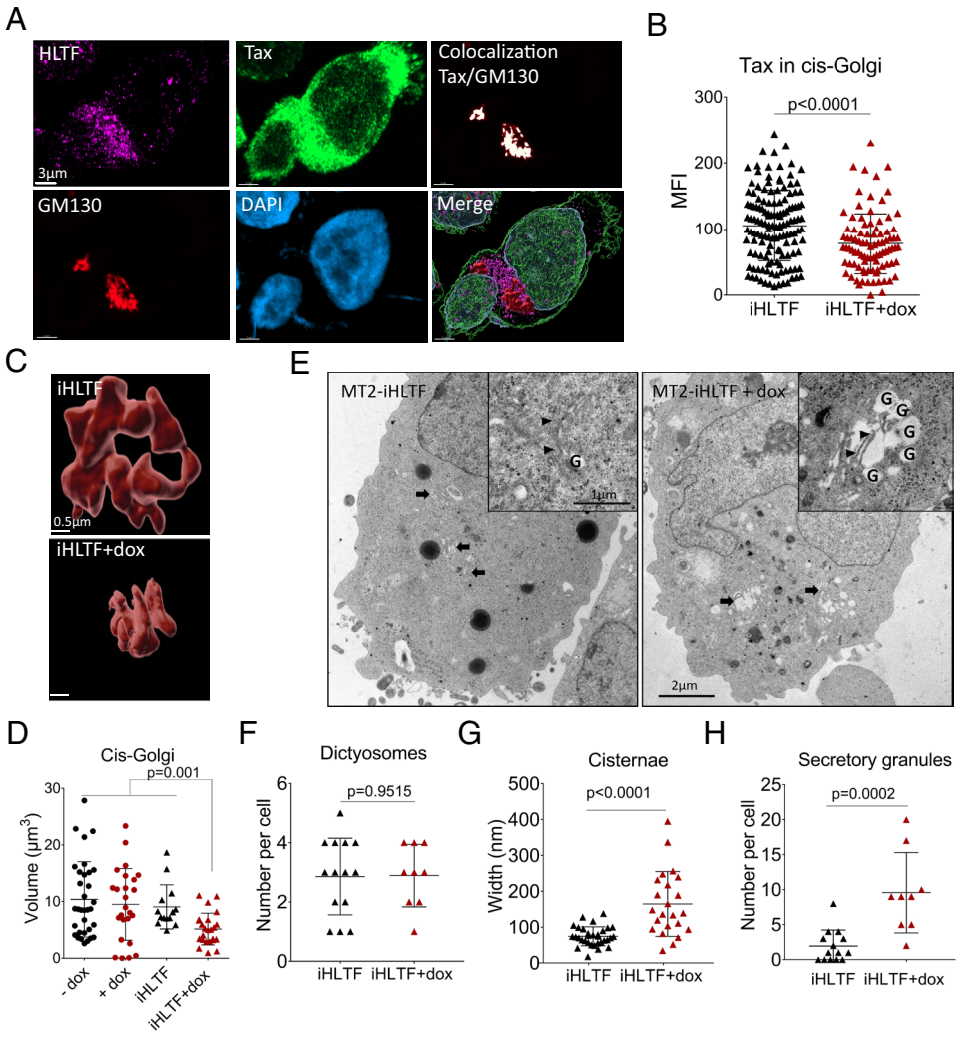

Fig. 4. Restoring normal levels of HLTF in HTLV-1-infected cell lines fragments the Golgi apparatus and increases granule secretion. (*A*) Confocal analysis of HLTF (pink, Texas Red), Tax (green, Alexa Fluor 488), GM130 (red, Alexa Fluor 647), and DAPI (blue) in MT2-iHLTF. Colocalization was determined with Zen Blue and Imaris software. (*B*) MFI of Tax protein in the cis-Golgi as identified with the anti-GM130 antibody in MT2-iHLTF cells after HLTF induction (+dox). The *P* value was calculated according to the Mann–Whitney test. (*C*) Confocal analysis of the cis-Golgi region (i.e., the cisternae nearest the endoplasmic reticulum) labeled by GM130 (red, Alexa Fluor 647) in MT2-iHLTF cells after HLTF induction (+dox). (*D*) Volume of the cis-Golgi region in MT2-iHLTF cells after HLTF induction. The volume of the cis-Golgi apparatus and voxel intensities were determined after a 3D-reconstructed confocal z-stacks of GM130 fluorescence using surface creation of Imaris. *P* values were calculated according to the Dunn's multiple comparison test. (*E*) Electron microscopy of MT2-iHLTF cells after HLTF induction (+dox) containing several dictyosomes (black arrows). Inserts show a dictyosome with these different cisternae (black arrowheads) at higher magnification. G are secretory granules. (*F*) Number of dictyosomes per cell in MT2-iHLTF cells with and without induction of HLTF (±dox). The *P* value was calculated according to the unpaired test (*G*) Cisternae width in MT2-iHLTF cells before and after HLTF induction (±dox). The *P* value was calculated according to the unpaired *t* test with Welch's correction. (*H*) Number of secretory granules per cell in MT2-iHLTF cells before and after HLTF induction (±dox). The *P* value was calculated according to the Mann–Whitney test.

number of dictyosomes (i.e., the stack of cisternae forming the Golgi apparatus) was not significantly affected by HLTF (black arrows in Fig. 4 *E* and *F*). However, the thickness of the cisternae (Fig. 4*E* inserts, black arrowheads) expanded 2.2-fold from 74.57 nm (±26.27) to 164.6 nm (±90.16) (*t* test with Welch's correction, $P < 0.0001$) (Fig. 4*G*). Concomitantly, the number of secretory granules per cell increased when HLTF was induced (Fig. 4*H*).

These results thus indicate that HLTF affects the Golgi apparatus organization and increases vesicle production in HTLV-1-infected cells.

HLTF Stimulates Tax-Mediated NF-κB Activation and Affects the Autophagic Flux. Since HLTF increased the number of secretory granules exiting the Golgi apparatus (Fig. 4 *E* and *H*), it was predicted that Tax-mediated NF-κB activation and autophagy may also be affected. By recruiting the IKK kinase complex to lipid rafts of the Golgi apparatus, Tax activates NF-κB and modulates the autophagy dynamics (34, 35). Because Tax stimulates autophagosome biogenesis and blocks autophagosome-lysosome fusion, this mechanism is essential for the viral life cycle (18, 36). To address this mechanism, Tax and HLTF were expressed in Hek293T cells using a doxycycline-inducible system. Adequate transcription and translation of Tax and HLTF were assessed by RT-qPCR (Fig. 5 *A* and *B*) and immunoblot assays (Fig. 5*C*), respectively. Activation of NF-κB was then quantified by lentiviral transduction of an NF-κB-luciferase reporter. Induction of Tax expression with doxycycline (iTax+dox) increased NF-κB signaling (Fig. 5*D*), consistently with previous reports (16). In similar conditions, HLTF alone had no effect (iHLTF+dox) but further stimulated the NF-κB pathway in the presence of Tax (iTaxiHLTF+dox) (Fig. 5*D*).

Tax connects the NF-κB pathway to autophagosome biogenesis via the BECN1/Bif-1/PI3KC3 complex (12). Tax promotes the formation of autophagosomes and concomitantly inhibits their fusion with lysosomes. To address this mechanism, the autophagic pathway

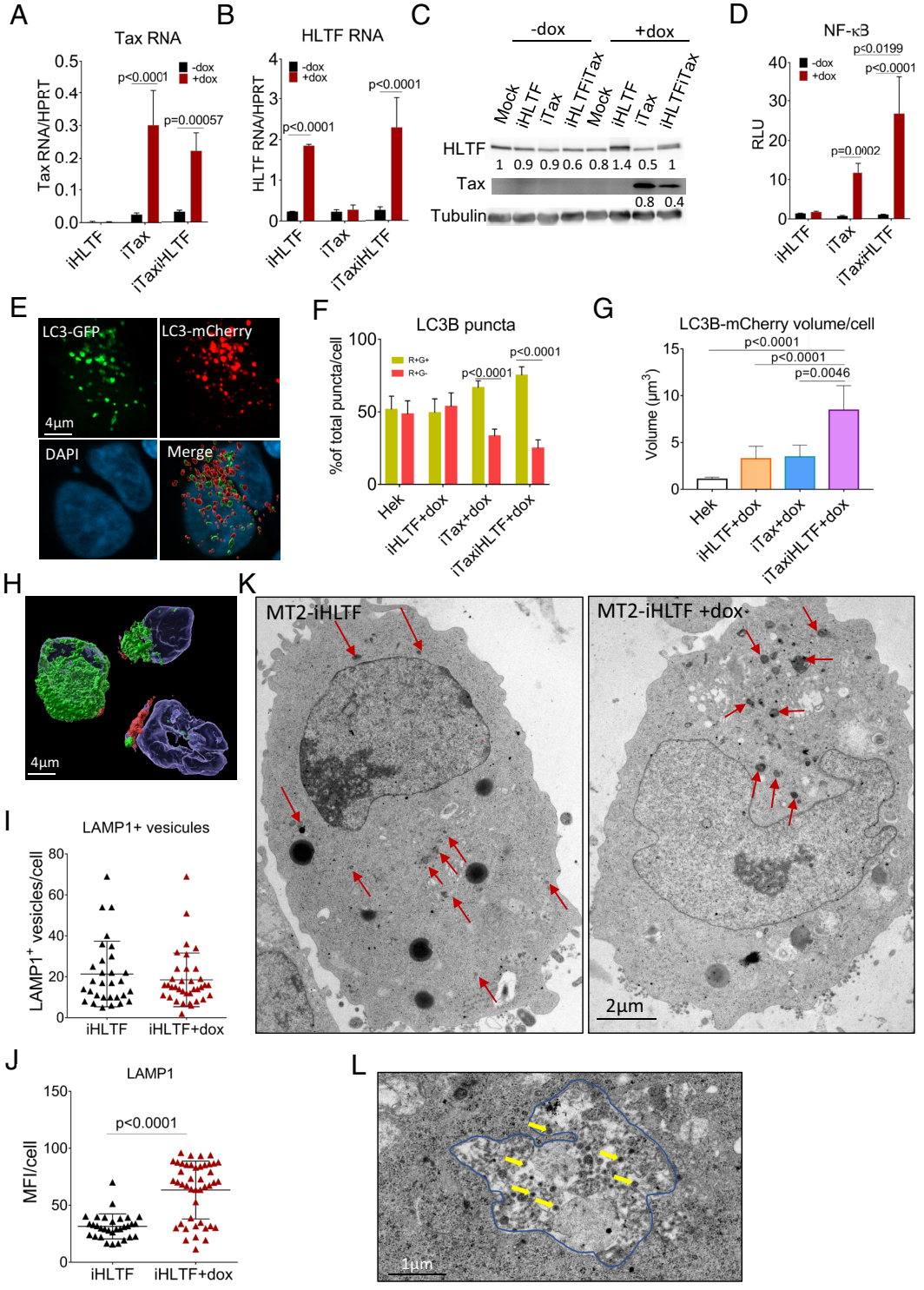

Fig. 5. HLTF synergizes with Tax to activate NF-κB signaling and affects the autophagic flux. (*A* and *B*) RT-qPCR of *tax* and *HLTF* RNAs in Hek293T cells after induction of Tax (iTax), HLTF (iHLTF) or both (iTaxiHLTF) with doxycycline (±dox). Data are presented as the mean (±SD) of at least three independent experiments. Statistical differences between ±dox for each condition (iHLTF, iTax, and iTaxiHLTF) were calculated according to *t* tests. (*C*) Western blot analysis of HLTF and Tax proteins in Hek293T cells after induction of Tax and/or HLTF. (*D*) Hek293T cells were transduced with a luciferase reporter vector to measure NF-κB activation. Relative luminescence units (RLU) are presented as the mean (±SD) of at least three independent experiments. Differences between ±dox for each condition (iHLTF, iTax, and iTaxiHLTF) were calculated according to *t* tests. (*E*) Confocal analysis of LC3B in Hek293T cells after transient transfection with the pBABE-puro-mCherry-EGFP-LC3B (*F*) Quantification of LC3B puncta per cell in Hek293T cells after induction of Tax and HLTF expression (+dox). Autophagosomes are positive for both fluorescent proteins (R+G+) while acidification in autolysosomes destroys EGFP emission (R+G−). Data are presented as the mean (±SEM) of at least three independent experiments. *P* values were calculated according to *t* tests. (G) Volume of LC3B-mCherry in Hek293T cells after Tax and HLTF expression. Data are presented as the mean (±SEM) of at least three independent experiments. *P* values were calculated according to Dunn's multiple comparison tests. (*H*) MT2 were labeled with Tax (green, Alexa Fluor 488) and the LAMP1 lysosomal marker (red, Alexa Fluor 647) upon induction of HLTF. Nuclei (DAPI) are in purple. (*I*) Percentages of LAMP1-positive puncta per cell. Data are presented as the mean (±SD) of at least three independent experiments. The Mann–Whitney test indicated that the datasets were not statistically different. (*J*) Data (MFI of LAMP1 per cell) are presented as the mean (±SD) of at least 3 independent experiments. *P* values were calculated according to the Mann–Whitney test. (*K* and *L*) Electron microscopy of lysosomes (red arrows) and viral particles (yellow arrows) in MT2-iHLTF cells after HLTF induction (+dox).

was analyzed with a retroviral vector expressing the LC3B marker fused to mCherry and EGFP (pBABE-puro-mCherry-EGFP-LC3B) (17). Using this vector, autophagosomes stained positive for both fluorescent proteins (R+G+) while acidification in autolysosomes destroyed EGFP emission (R+G–) (Fig. 5*E*). The percentages of red puncta per cell decreased in Hek293T cells transduced with a Tax lentivector in the presence of doxycycline (Fig. 5*F*). This observation confirms previous reports showing that Tax inhibits the fusion of autophagosomes with lysosomes (12, 17). Coexpression of Tax and HLTF did not significantly modify the ratio between R+G+ and R+G– puncta. However, the R+G– volume per cell significantly increased in the presence of HLTF and Tax (Fig. 5*G*), indicating that the lysosomes became larger.

To further extend these conclusions to HTLV-1-infected cells, MT2 cells were labeled with the LAMP1 lysosomal marker upon induction of HLTF (LAMP1 in red and Tax in green in Fig. 5*H*). The percentage of LAMP1-positive puncta per cell was not modified (Fig. 5*I*) but the MFI/cell significantly increased (Fig. 5*J*). Transmission electron microscopy revealed that upon induction of HLTF, large lysosomes (~1 mm) appeared in the peri-Golgi area (red arrows, Fig. 5*K*). Concomitantly, large autolysosomes containing numerous viral particles formed in the presence of HLTF (yellow arrows, Fig. 5*L*). Note that all these experiments were performed in conditions of physiologically relevant levels of HLTF expression (Fig. 1*I*).

Together these results demonstrate that HLTF does not affect the ability of Tax to block autophagosome-lysosome fusion. However, the coexpression of Tax and HLTF exacerbates the vesicular trafficking leading to an enlargement of the lysosomes and the production of large autolysosomes containing viral particles.

HLTF Induction Increases the Number of Defective Virions and Restricts HTLV-1 Infectivity in Primary Lymphocytes. Increased granule secretion in the Golgi apparatus (Fig. 4) combined with the enlargement of lysosomes (Fig. 5) is predicted to affect the infectious cycle of HTLV-1. To study virus transmission through the virological synapse, HTLV-1-infected MT2 lymphocytes were cocultured with noninfected Jurkat T cells and imaged by confocal microscopy. Clustering of the lymphocyte function-associated antigen 1 (LFA-1, integrin alpha, CD11a) at the cell contact sites indicated the genesis of a virological synapse (37) (Fig. 6*A*). When HLTF was induced in MT2 cells, the colocalization of Tax, HLTF, and CD11a was slightly reduced although this trend approached but did not reach statistical significance (P=0.0741 according to the Mann–Whitney test) (Fig. 6*B*). Careful examination of the viral particles by transmission electron microscopy highlighted a major change in the structure of the virions (Fig. 6*C*). The percentage of enveloped particles containing electron-dense cores decreased from 19.0 to 11.3% (Fig. 6*C*). The mean diameter of the virions very significantly increased in the presence of HLTF (from 69.8 to 76.6 nm; $P < 0.0001$ according to the t test) (Fig. 6*C*). This change in the virion size has been associated with immature viral particles devoid of fully processed capsids complexed with the genomic RNA (38, 39).

To further validate this conclusion, the particle distribution was determined in the cell culture supernatant using a molecular size analyzer (Zetasizer Nano ZS, Malvern Instruments). Induction of HLTF reduced the proportion of ~100 nm particles expressed by MT2-iHLTF cells (blue arrows on Fig. 6*D*). In contrast, the profile of exosomes was unaffected by HLTF (*SI Appendix*, Fig. S13).

Together, these results show that physiologically relevant levels of HLTF promote the release of defective viral particles by HTLV-1-infected cells. To further sediment this conclusion, we analyzed the capacity of MT2 cells to transduce virus to normal lymphocytes upon HLTF induction. Lymphocytes from five healthy donors were isolated from the peripheral blood, labeled with CFSE, and cocultured with γ-irradiated MT2-iHLTF for 10 d (Fig. 6*E*). As illustrated in Fig. 6*F*, the percentages of Tax+CFSE+ lymphocytes decreased from 30 to 20% when HLTF was induced in MT2 (lymphocytes + MT2 – iHLTF). This infectivity assay indicated that HLTF also restricted early steps of HTLV-1 infection, as demonstrated for HIV (40). Using normal lymphocytes isolated from 5 different healthy donors, the difference was statistically significant (Fig. 6*G*).

Confocal microscopy analysis of the primary cultures revealed that HLTF expression was induced in CFSE+ lymphocytes staining positive for Tax used here as a marker of HTLV-1 infection (see arrows in Fig. 6*H*). Tax and HLTF colocalized in discrete speckles in newly infected primary lymphocytes (Fig. 6*I*), supporting the biological relevance of their interaction. A spatial colocalization of Tax and HLTF was also observed in transiently cultured PBMCs isolated from ATL patients (*SI Appendix*, Fig. S14 *A* and *B*). In these ATL cell cultures, Tax expression was heterogenous, consistently with reports from the literature (27). In the fraction of Tax+ cells, the MFI of HLTF was increased (from MFI 432 in Tax– to MFI 1032 in Tax+; *SI Appendix*, Fig. S14*C*), as observed in newly infected lymphocytes (Fig. 6*H*). After coculture of ATL PBMCs and CFSE-labeled primary lymphocytes from two healthy donors, expression of HLTF increased (*SI Appendix*, Fig. S14*D*), consistently with a model of HLTF-dependent restriction at early steps of infection.

In summary, these results show that (i) the capacity of MT2 cells to transduce virus to normal lymphocytes is restricted by HLTF, (ii) Tax and HLTF colocalize in discrete speckles in newly infected primary lymphocytes and ATL PBMCs, and (iii) HLTF expression is induced at early steps of viral infection. These data thus support the biological relevance of HLTF as a restriction factor in primary lymphocytes.

Discussion

In this report, we showed that HLTF is a restriction factor that limits cell-to-cell infection by HTLV-1 at early and late steps of the viral life cycle. The biological relevance of HLTF in viral replication and pathogenesis is supported by the analysis of HLTF expression in patients' samples (Fig. 1). Transcription of *HLTF* is indeed significantly reduced in HAM/TSP and ATL subjects compared to healthy donors and asymptomatic carriers. In relevant cell culture models, the *HLTF* transcription is impaired by the EZH2 chromatin methyltransferase and by cytosine methylation of the gene promoter (*SI Appendix*, Figs. S3 and S4). Besides transcriptional inhibition, the Tax protein interacts with and binds HLTF for proteosomal degradation (Fig. 2). These three inhibitory levels of HLTF expression further support its key role in HTLV replication. Modulation by RNA interference and gene transduction demonstrates that HLTF acts as a restriction factor in HTLV-1-infected cell lines (Fig. 3 and *SI Appendix*, Fig. S10).

The mechanism of HLTF restriction involves a dysregulation of the vesicular trafficking from the Golgi apparatus (Fig. 4). When normal levels of HLTF expression are restored in HTLV-1-infected cells, the Golgi cisternae enlarge and the number of secretory granules increases. This process does not affect the ability of Tax to inhibit autophagosome-lysosome fusion (Fig. 5). The consequence of Golgi fragmentation and increased vesicular trafficking is an enlargement of the lysosome. Overall, this results in the production of immature viral particles (Fig. 6). The spatial colocalization and infectivity assays with ATL PBMCs and primary lymphocytes

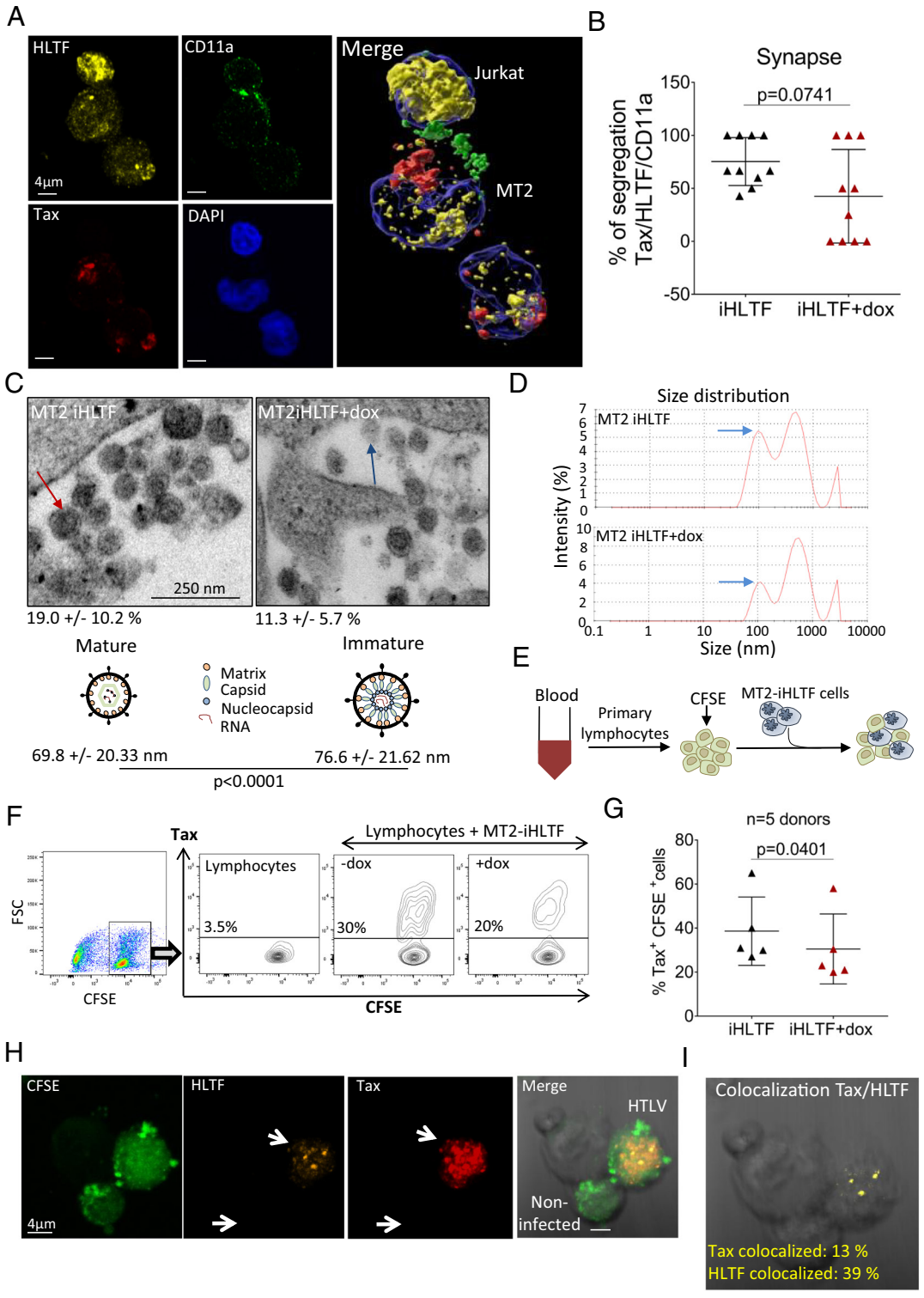

Fig. 6. Physiological levels of HLTF induce immature viral particles and reduce HTLV-1 infectivity in primary T cells. (*A*) Confocal analysis of DAPI (blue), CD11a (green, Alexa Fluor 488), Tax (red, Alexa Fluor 647), and HLTF (yellow, Texas red) in cocultures of Jurkat and MT2 cells. (*B*) Segregation of Tax, HLTF, and CD11a at contact sites of Jurkat and MT2-iHLTF conjugates using Zen Blue and Imaris software. *P* values were calculated according to the Mann–Whitney test. (*C*) Transmission electron microscopy imaging of MT2-iHLTF cells before (MT2iHLTF) and after HLTF induction (MT2iHLTF +dox). Red and blue arrows represent mature and immature particles, respectively. In the bottom panels, the mature and immature particles are represented schematically. In a mature particle (*Left*), the nucleocapsid (blue) forms a complex with the viral RNA (red), and the capsid (green) is surrounded by the matrix protein (orange). In an immature protein (*Right*), the nucleocapsid and the viral genomic RNA are not complexed, and the capsid is not formed. The percentages of enveloped viral particles are indicated (% ±SD). Numbers (nm ± SD) correspond to the mean diameters of viral particles after HLTF induction. The *P* value was calculated according to the *t* test. (*D*) Size distribution of particles in the supernatant of MT2-iHLTF cells before and after HLTF induction with doxycycline. The arrow indicates the fractions containing the ~100 nm particles. A representative experiment out of 4 is shown. (*E*) Primary lymphocytes were labeled with CFSE and cocultured for 10 d at a 1:1 ratio with γ-irradiated (10 Gy) MT2-iHLTF. (*F*) Cells were labeled with an antibody directed against Tax and an Alexa Fluor 647 conjugate. Newly infected Tax+CFSE+ cells were analyzed by flow cytometry. A representative experiment out of 5 is shown. (*G*) Quantification of Tax+CFSE+ cells in cocultures of MT2-iHLTF with lymphocytes from five donors. *P* values were calculated according to the *t* test. (*H*) Tax (Alexa Fluor 647, red) and HLTF (Texas red, orange) were analyzed by confocal microscopy. (*I*) Colocalization of Tax and HLTF in a newly infected lymphocyte. The threshold for colocalization was set manually. The numbers indicate the percentages of Tax and HLTF that colocalize with HLTF and Tax, respectively.

support the biological relevance of HLTF as a restriction factor in vivo (Fig. 6 and *SI Appendix*, Fig. S14).

Together, these results highlight a complex dynamic equilibrium between different secretory pathways that are required for adequate production of infectious viral particles (Fig. 7). Of note, mature HTLV-1 virions are quite heterogeneous (113 ± 23 nm) based on cryo-TEM (41). Our analysis of thinner sections by TEM (Fig. 6) consistently yielded lower but still heterogeneous values (69.8 ± 20.33 nm). In fact, HTLV-1-infected cells express a broad spectrum of noninfectious virions, mature particles, and extracellular vesicles (42). Differential ultracentrifugation identified different types of vesicles containing viral proteins (p19, Tax), autophagy components (LC3 and p62), cytokines (IL18 and IL-33), and even, core histones. Whether HLTF affects the number and/or the composition of these extracellular vesicles remains to be determined. Our data of *SI Appendix*, Fig. S13, nonetheless indicated that the exosomes appear to be unaffected in the presence of HLTF. Another interesting issue is the kinetics that mediates the mutual exclusion of Tax and HLTF expression (Fig. 2 *J* and *K*). Expression of Tax is indeed heterogeneous in primary HTLV-1-infected T cell clones and fluctuates in intermittent bursts in the absence of HBZ (27). Conceptually, it is therefore predicted that a transient increase in Tax levels would impair HLTF transcription and induce its proteasomal degradation. Conversely, reduced Tax expression would restore HLTF levels and promote viral restriction. This model is consistent with a dynamic role of Tax in viral persistence and ATL maintenance (43).

The HLTF protein has a rather unusual structure combining apparently unrelated activities: DNA binding, ATP-dependent nucleosome remodeling, and E3 ubiquitin ligase (44). HLTF is a translocase that regulates fork reversal in the DNA damage tolerance pathways. HLTF inhibits early steps of cell entry by other viruses such as human cytomegalovirus (hCMV) and HIV. By promoting proteasomal degradation, hCMV UL145 and HIV Vpr counteract HLTF-mediated restriction (40, 45–47). HLTF also inhibits early HTLV-1 infection when expressed in recipient Jurkat T cells (*SI Appendix*, Fig. S10), highlighting conserved restriction pathways shared by different viruses. The restriction mechanism that we have described here occurs at later steps in the cell that is persistently infected by HTLV-1. HLTF activates Tax-dependent NF-κB signaling, fragments the Golgi apparatus, and enlarges lysosomes (Fig. 5). The mechanism involved in HLTF restriction within persistently infected HTLV-1 cells also differs from that of Tetherin/BST-2. This transmembrane protein potently anchors budding viral particles at the cell membrane, preventing the release of HIV-1 (48). In contrast, HLTF-dependent restriction of HTLV-1 is mediated by the autophagic flux (Fig. 5). Another important restriction factor of HIV is the E3 ubiquitin ligase TRIM5α which blocks viral replication immediately after entry and prior to integration. TRIM5α targets the viral capsid and prevents the uncoating of the viral preintegration complex (49). The E3 ubiquitin ligase activity associated with the RING domain of TRIM5α is required for degradation of the HIV-1 capsid in the proteasome. Whether this mechanism also applies to HLTF-mediated restriction of HTLV-1 early infection remains to be determined.

This report thus contributes to a better understanding of the viral restriction of the HTLV-1 replication cycle. Relatively few restriction factors of HTLV-1 have been identified and their modes of action are still unclear and sometimes controversial (3, 6).

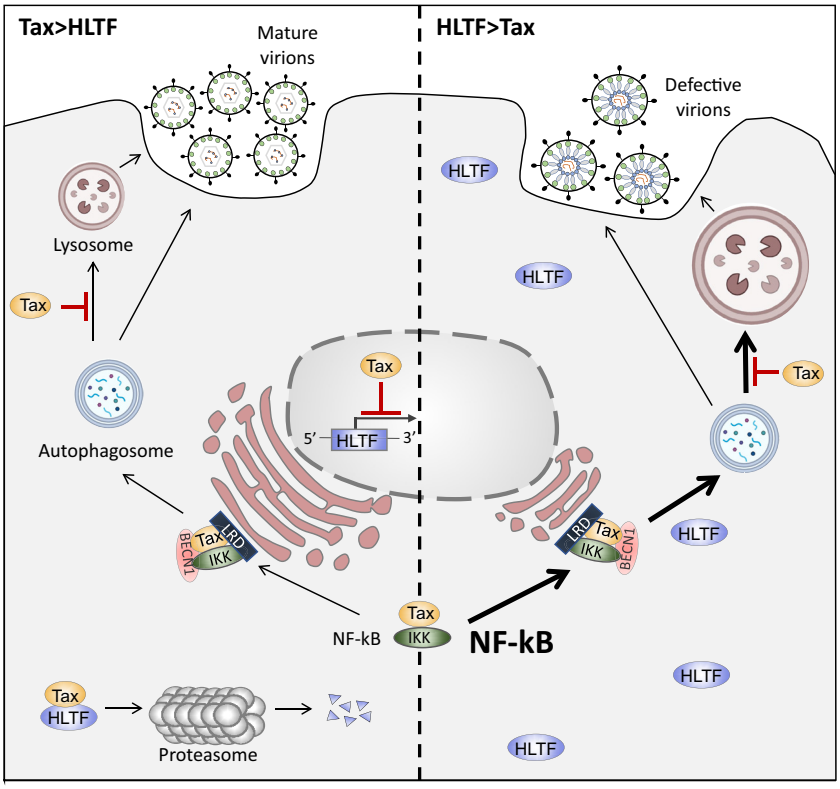

Fig. 7. A model of HLTF-mediated restriction. The levels of Tax fluctuate in HTLV-1-infected lymphocytes (27). In cells expressing Tax (Tax>HLTF), HLTF transcription is inhibited via the EZH2 methyltransferase. The Tax protein directly interacts with HLTF and induces its proteasomal degradation. Tax activates NF-κB signaling and inhibits autophagosome fusion with lysosomes. Promotion of autophagy at the expense of lysosomal proteolysis favors the release of mature viral particles. Restoring HLTF levels (HLTF>Tax) overactivates the NF-κB pathway, fragments the Golgi apparatus, and produces large autolysosomes containing viral particles. As a consequence, HLTF increases the number of immature virions, thereby restricting HTLV-1 infection.

Restoration of physiologically relevant levels of HLTF expression in lymphocytes derived from patients drastically modifies the secretory pathways. In particular, the Golgi morphology is critically regulated by proteasomal degradation after a stress-induced activation (50). The ubiquitination of the Golgi tethering factors GM130 and GRASP65 controls the morphology of the organelle. Degradation of these structural factors leads to GARD. Under Golgi-stress conditions, activation of GARD leads to cell death in multiple myeloma likely due to their extended secretory system (50). In HTLV-1-infected lymphocytes, apoptotic events occurred upon Golgi dispersal but concerned only a relatively small fraction of cells. Instead, the stress likely associated with NF-κB overactivation induced by the synergistic action of HLTF and Tax leads to the secretion of large autophagic vacuoles containing viral particles (Fig. 5). These autophagosomes are predicted to undergo a maturation process after fusion with endosomes to generate amphisomes (51). Indeed, formation of these intermediate organelles is an essential step during a sequential maturation process of autophagosomes before their ultimate fusion with lysosomes for cargo degradation. Amphisomes can either fuse with lysosomes for subsequent degradation or be exported to the plasma membrane for secretion. The present work reveals that Tax still inhibits autophagosome-lysosome fusion (Fig. 5) and that the proportion of mature virions in the supernatant is reduced (Fig. 6). It is however likely that the Golgi fragmentation is responsible for the enlargement of the lysosomes, indicating that the ability of Tax to inhibit autophagosome-lysosome fusion is overwhelmed or bypassed. Lysosomes respond rapidly to a broad diversity of intra- and extracellular stimuli triggering structural changes (52). The numbers, size, and position of lysosomes mediate their activity and influence cell homeostasis. In particular, increased lysosomal size negatively influences exocytosis and is associated with a number of disease conditions (52, 53). The dynamics of these structural changes of the lysosomes in HTLV-1 restriction by HLTF clearly merit further investigation.

In conclusion, this report highlights a mechanism of restriction based on the ability of HLTF to overactivate Tax-dependent NF-κB-mediated autophagy. Stress-induced Golgi fragmentation, excessive release of secretory granules, lysosomal enlargement, and ultimately the decrease of viral infectivity recapitulates the mechanisms of HLTF-mediated restriction.

Materials and Methods

SI Appendix contains the description of HTLV-1-infected cell lines as well as the isolation of ATL PBMCs and primary lymphocytes. It also describes the different methods: luciferase reporter tests, GPCA, RT-qPCR, immunoblotting, coimmunoprecipitation, immunofluorescence and confocal microscopy, transmission electron microscopy, single-cycle infectivity assay, quantification of particle distributions in cell culture supernatants, and infectivity assays with primary lymphocytes and statistics.

Data, Materials, and Software Availability. All study data are included in the article and/or *SI Appendix*.

ACKNOWLEDGMENTS. This work was supported by research credit (CDR J.0195.21), research project (PDR T.0261.20), and Télévie grants from the Belgian National Fund for Scientific Research (FNRS). Additional support was obtained from the "Commission permanente facultaire à la recherche" and the "Fonds Spéciaux pour la Recherche" (University of Liège), the Belgian Foundation against Cancer, and the Léon Fredericq Foundation. A.B. (research fellow) and L.W. (research director) are members of the FNRS. H.G., P.S.C., M.J., and M.H. received postdoctoral grants from the Télévie and the Belgian Foundation against Cancer. We are grateful to Renaud Mahieux and Françoise Bex for providing cell lines.

Author affiliations: [a]Laboratory of Molecular and Cellular Epigenetics, Grappe Interdisciplinaire de Génoprotéomique Appliquée, University of Liège, 4000, Liège, Belgium; [b]Molecular Biology, Teaching and Research Center, University of Liège, 5030, Gembloux, Belgium; [c]Laboratory of Cell and Tissue Biology, Grappe Interdisciplinaire de Génoprotéomique Appliquée, University of Liège, 4000, Liège, Belgium; [d]Laboratory of Molecular Immunology & Signal Transduction, Grappe Interdisciplinaire de Génoprotéomique Appliquée, University of Liège, 4000, Liège, Belgium; [e]Viral Vectors Platform, Grappe Interdisciplinaire de Génoprotéomique Appliquée, University of Liège, 4000 Liège, Belgium; [f]Laboratory of Viral Interactomes, Unit of Molecular Biology of Diseases, Grappe Interdisciplinaire de Génoprotéomique Appliquée, University of Liège, 4000 Liège, Belgium; [g]Institut de Recherche en Infectiologie de Montpellier, Université de Montpellier, CNRS, 34094, Montpellier, France; [h]Laboratory of Pneumology, Grappe Interdisciplinaire de Génoprotéomique Appliquée, University of Liège, University Hospital of Liège, 4000 Liège, Belgium; and [i]Department of Hematology, Kumamoto University, 860-8556, Kumamoto, Japan

1. V. M. Zhdanov, F. I. Yershov, L. V. Uryvayev, D. I. Ivanovsky, Formation of infectious arbovirus ribonucleoprotein in subcellular structures. *Nature* **228**, 1192–1194 (1970).
2. J. Boeke, J. Stoye, "Retrotransposons, Endogenous Retroviruses, and the Evolution of Retroelements" in *Retroviruses* (Cold Spring Harbor Laboratory Press, 1997), pp. 343–435.
3. G. Forlani, M. Shallak, E. Ramia, A. Tedeschi, R. S. Accolla, Restriction factors in human retrovirus infections and the unprecedented case of CIITA as link of intrinsic and adaptive immunity against HTLV-1. *Retrovirology* **16**, 1–12 (2019).
4. R. Farrukee, M. Ait-Goughoulte, P. M. Saunders, S. L. Londrigan, P. C. Reading, Host cell restriction factors of paramyxoviruses and pneumoviruses. *Viruses* **12**, 1381 (2020).
5. C. Chamontin, G. Bossis, S. Nisole, N. J. Arhel, G. Maarifi, Regulation of viral restriction by post-translational modifications. *Viruses* **13**, 2197 (2021).
6. A. Carcone, C. Journo, H. Dutartre, Is the HTLV-1 retrovirus targeted by host restriction factors? *Viruses* **14**, 1611 (2022).
7. M. Colomer-Lluch, A. Ruiz, A. Moris, J. G. Prado, Restriction factors: From intrinsic viral restriction to shaping cellular immunity against HIV-1. *Front. Immunol.* **9**, 2876 (2018).
8. M. Mansouri *et al.*, Molecular mechanism of BST2/tetherin downregulation by K5/MIR2 of Kaposi's sarcoma-associated herpesvirus. *J. Virol.* **83**, 9672–9681 (2009).
9. Y. Iwabu *et al.*, HIV-1 accessory protein Vpu internalizes cell-surface BST-2/Tetherin through transmembrane interactions leading to lysosomes. *J. Biol. Chem.* **284**, 35060–35072 (2009).
10. R. Benyair, A. Eisenberg-Lerner, Y. Merbl, Maintaining golgi homeostasis: A balancing act of two proteolytic pathways. *Cells* **11**, 780 (2022).
11. T. Vescovo, B. Pagni, M. Piacentini, G. M. Fimia, M. Antonioli, Regulation of autophagy in cells infected with oncogenic human viruses and its impact on cancer development. *Front. cell Dev. Biol.* **8**, 47 (2020).
12. N. Ducasa *et al.*, Autophagy in human T-cell leukemia virus type 1 (HTLV-1) induced leukemia. *Front. Oncol.* **11**, 967 (2021).
13. N. M. Kocaturk, D. Gozuacik, Crosstalk between mammalian autophagy and the ubiquitin-proteasome system. *Front. Cell Dev. Biol.* **6**, 128 (2018).
14. H. Y. Winter, S. J. Marriott, Human T-cell leukemia virus type 1 tax enhances serum response factor DNA binding and alters site selection. *J. Virol.* **81**, 6089–6098 (2007).
15. K. T. Jeang, Functional activities of the human T-cell leukemia virus type I Tax oncoprotein: Cellular signaling through NF-kappa B. *Cytokine Growth Factor Rev.* **12**, 207–217 (2001).
16. X. H. Li, R. B. Gaynor, Regulation of NF-κB by the HTLV-1 Tax Protein. *Gene Expr.* **7**, 233–245 (1999).
17. S.-W. Tang, C.-Y. Chen, Z. Klase, L. Zane, K.-T. Jeang, The cellular autophagy pathway modulates human T-cell leukemia virus type 1 replication. *J. Virol.* **87**, 1699–1707 (2013).
18. T. Ren *et al.*, HTLV-1 Tax deregulates autophagy by recruiting autophagic molecules into lipid raft microdomains. *Oncogene* **34**, 334–345 (2015).
19. Y.-K. Ho *et al.*, HTLV-1 Tax stimulates ubiquitin E3 Ligase, ring finger protein 8, to assemble lysine 63-linked polyubiquitin chains for TAK1 and IKK activation. *PLoS Pathog.* **11**, e1005102 (2015).
20. Y. Shibata *et al.*, HTLV-1 Tax induces formation of the active macromolecular IKK complex by generating Lys63- and Met1-linked hybrid polyubiquitin chains. *PLoS Pathog.* **13**, e1006162 (2017).
21. S. Mohanty *et al.*, The E3/E4 ubiquitin conjugation factor UBE4B interacts with and ubiquitinates the HTLV-1 Tax oncoprotein to promote NF-κB activation. *PLoS Pathog.* **16**, e1008504 (2020).
22. A. Schwob *et al.*, SQSTM-1/p62 potentiates HTLV-1 Tax-mediated NF-κB activation through its ubiquitin binding function. *Sci. Rep.* **9**, 1–17 (2019).
23. R. G. Andrade *et al.*, Strong correlation between tax and HBZ mRNA expression in HAM/TSP patients: Distinct markers for the neurologic disease. *J. Clin. Virol.* **56**, 135–140 (2013).
24. Y. Yamano *et al.*, Correlation of human T-cell lymphotropic virus type 1 (HTLV-1) mRNA with proviral DNA load, virus-specific CD8(+) T cells, and disease severity in HTLV-1-associated myelopathy (HAM/TSP). *Blood* **99**, 88–94 (2002).
25. S. Takeda *et al.*, Genetic and epigenetic inactivation oftax gene in adult T-cell leukemia cells. *Int. J. Cancer* **109**, 559–567 (2004).
26. G. Belrose *et al.*, Effects of valproate on Tax and HBZ expression in HTLV-1 and HAM/TSP T lymphocytes. *Blood* **118**, 2483–2491 (2011).
27. M. R. Billman, D. Rueda, C. R. M. Bangham, Single-cell heterogeneity and cell-cycle-related viral gene bursts in the human leukaemia virus HTLV-1. *Wellcome Open Res.* **2**, 87 (2017).
28. D. Fujikawa *et al.*, Polycomb-dependent epigenetic landscape in adult T-cell leukemia. *Blood* **127**, 1790–1802 (2016).
29. P. Cassonnet *et al.*, Benchmarking a luciferase complementation assay for detecting protein complexes. *Nat. Methods* **8**, 990–992 (2011).
30. M. Mahgoub *et al.*, Sporadic on/off switching of HTLV-1 Tax expression is crucial to maintain the whole population of virus-induced leukemic cells. *Proc. Natl. Acad. Sci. U.S.A.* **115**, E1269–E1278 (2018).
31. R. Rousset, C. Desbois, F. Bantignies, P. Jalinot, Effects on NF-kappa B1/p105 processing of the interaction between the HTLV-1 transactivator Tax and the proteasome. *Nature* **381**, 328–331 (1996).

32. S. Alais, H. Dutartre, R. Mahieux, Quantitative analysis of human T-Lymphotropic virus type 1 (HTLV-1) infection using co-culture with jurkat LTR-Luciferase or Jurkat LTR-GFP reporter cells. *Methods Mol. Biol.* **1582**, 47–55 (2017).
33. G. Bai *et al.*, HLTF Promotes fork reversal, limiting replication stress resistance and preventing multiple mechanisms of unrestrained DNA synthesis. *Mol. Cell* **78**, 1237–1251.e7 (2020).
34. Z. L. Chu, J. A. DiDonato, J. Hawiger, D. W. Ballard, The tax oncoprotein of human T-cell leukemia virus type 1 associates with and persistently activates IkappaB kinases containing IKKalpha and IKKbeta. *J. Biol. Chem.* **273**, 15891–15894 (1998).
35. A. Criollo *et al.*, The IKK complex contributes to the induction of autophagy. *EMBO J.* **29**, 619–631 (2010).
36. J. Huang, T. Ren, H. Guan, Y. Jiang, H. Cheng, HTLV-1 Tax is a critical lipid raft modulator that hijacks IkappaB kinases to the microdomains for persistent activation of NF-kappaB. *J. Biol. Chem.* **284**, 6208–6217 (2009).
37. S. Kim, A. M. Nair, S. Fernandez, L. Mathes, M. D. Lairmore, Enhancement of LFA-1-mediated T cell adhesion by human T lymphotropic virus Type 1 p12I1. *J. Immunol.* **176**, 5463–5470 (2006).
38. I. F. Grigsby *et al.*, Biophysical analysis of HTLV-1 particles reveals novel insights into particle morphology and Gag stochiometry. *Retrovirology* **7**, 1–13 (2010).
39. I. Miyoshi *et al.*, Type C virus particles in a cord T-cell line derived by co-cultivating normal human cord leukocytes and human leukaemic T cells. *Nature* **294**, 770–771 (1981).
40. J. Yan, M. C. Shun, Y. Zhang, C. Hao, J. Skowronski, HIV-1 Vpr counteracts HLTF-mediated restriction of HIV-1 infection in T cells. *Proc. Natl. Acad. Sci. U.S.A.* **116**, 9568–9577 (2019).
41. J. O. Maldonado, S. Cao, W. Zhang, L. M. Mansky, Distinct morphology of human T-cell leukemia virus Type 1-like particles. *Viruses* **8**, 132 (2016).
42. D. O. Pinto *et al.*, Extracellular vesicles from HTLV-1 infected cells modulate target cells and viral spread. *Retrovirology* **18**, 1–27 (2021).
43. A. Bazarbachi, Tax fingerprint in adult T-cell leukemia. *Blood* **127**, 1737–1738 (2016).
44. Y. J. Achar *et al.*, Human HLTF mediates postreplication repair by its HIRAN domain-dependent replication fork remodelling. *Nucleic Acids Res.* **43**, 10277–10291 (2015).
45. H. Lahouassa *et al.*, HIV-1 Vpr degrades the HLTF DNA translocase in T cells and macrophages. *Proc. Natl. Acad. Sci. U.S.A.* **113**, 5311–5316 (2016).
46. K. Hrecka *et al.*, HIV-1 and HIV-2 exhibit divergent interactions with HLTF and UNG2 DNA repair proteins. *Proc. Natl. Acad. Sci. U.S.A.* **113**, E3921–E3930 (2016).
47. K. Nightingale *et al.*, High-definition analysis of host protein stability during human cytomegalovirus infection reveals antiviral factors and viral evasion mechanisms. *Cell Host. Microbe* **24**, 447–460.e11 (2018).
48. A. Presle *et al.*, The viral restriction factor tetherin/BST2 tethers cytokinetic midbody remnants to the cell surface. *Curr. Biol.* **31**, 2203–2213.e5 (2021).
49. A. P. M. Cloherty, A. G. Rader, B. Compeer, C. M. S. Ribeiro, Human TRIM5α: Autophagy connects cell-intrinsic HIV-1 restriction and innate immune sensor functioning. *Viruses* **13**, 320 (2021).
50. A. Eisenberg-Lerner *et al.*, Golgi organization is regulated by proteasomal degradation. *Nat. Commun.* **11**, 409 (2020).
51. D. Ganesan, Q. Cai, Understanding amphisomes. *Biochem. J.* **478**, 1959–1976 (2021).
52. M. E. G. de Araujo, G. Liebscher, M. W. Hess, L. A. Huber, Lysosomal size matters. *Traffic* **21**, 60–75 (2020).
53. C. Huynh, D. Roth, D. M. Ward, J. Kaplan, N. W. Andrews, Defective lysosomal exocytosis and plasma membrane repair in Chediak-Higashi/beige cells. *Proc. Natl. Acad. Sci. U.S.A.* **101**, 16795–16800 (2004).